Propagating elastic vibrations dominate thermal conduction in amorphous silicon

Jaeyun Moon, Benoit Latour, and Austin J. Minnich*

Division of Engineering and Applied Science, California Institute of Technology, Pasadena, California 91125, USA

(Received 26 April 2017; revised manuscript received 15 December 2017; published 10 January 2018)

The thermal atomic vibrations of amorphous solids can be distinguished by whether they propagate as elastic waves or do not propagate due to lack of atomic periodicity. In a-Si, prior works concluded that nonpropagating waves are the dominant contributors to heat transport, with propagating waves being restricted to frequencies less than a few THz and scattered by anharmonicity. Here, we present a lattice and molecular dynamics analysis of vibrations in a-Si that supports a qualitatively different picture in which propagating elastic waves dominate the thermal conduction and are scattered by local fluctuations of elastic modulus rather than anharmonicity. We explicitly demonstrate the propagating nature of waves up to around 10 THz, and further show that pseudoperiodic structures with homogeneous elastic properties exhibit a marked temperature dependence characteristic of anharmonic interactions. Our work suggests that most heat is carried by propagating elastic waves in a-Si and demonstrates that manipulating local elastic modulus variations is a promising route to realize amorphous materials with extreme thermal properties.

DOI: 10.1103/PhysRevB.97.024201

I. INTRODUCTION

Amorphous materials are of interest for a wide range of applications due to their low thermal conductivity [1,2]. While in crystals heat is carried by propagating lattice waves, or phonons, in amorphous solids heat carriers are classified as propagons, diffusons, and locons depending on the degree of delocalization of the atomic vibrations and their mean free paths [3,4].

This classification has been widely used to analyze the vibrations responsible for thermal transport in amorphous materials, especially for pure a-Si. Numerical studies using equilibrium molecular dynamics (EMD) and lattice dynamics (LD) have attempted to determine the fraction of heat carried by each category of vibration [5,6]. While the general consensus is that diffusons carry the majority of the heat, prior works have reported that propagons may carry 20%–50% of thermal conductivity in a-Si due to their long mean free paths [3,5]. Using normal-mode analysis, Larkin and McGaughey reported that propagons have a lifetime scaling of ω^{-2} which suggests plane-wave-like propagation that is not affected by atomic disorder [6]. The normal mode lifetime analysis of Lv and Henry concluded that the phonon gas model is not applicable to amorphous materials [7]. Experimental works have qualitatively confirmed some of these predictions, particularly regarding the important contribution of propagons [8–13]. For instance, Kwon *et al.* observed size effects in a-Si nanostructures, indicating the presence of propagons [12].

Despite these efforts, numerous puzzles remain. One discrepancy concerns the conclusion that the lifetimes of few THz vibrations are governed by anharmonicity [6]. If that is the case, explaining the low thermal conductivity of a-Si is challenging because the same vibrations contribute 75 W $m^{-1}K^{-1}$ to thermal conductivity in c-Si. Accounting for the low thermal conductivity of a-Si only by changes in anharmonicity requires either large increases in anharmonic force constants or in the scattering phase space. These changes would in turn affect other properties like the heat capacity of a-Si that have not been observed [10]. Along similar lines, if lifetimes of few THz vibrations are governed by anharmonicity the reported thermal conductivities of films of the same thickness should be reasonably uniform, yet the data vary widely [8,10,13]. Overall, an unambiguous classification of the propagating nature and scattering mechanisms of vibrational modes transporting heat in amorphous solids is poorly developed, impeding efforts to synthesize, for example, novel materials with exceptionally low thermal conductivity.

In this work, we address these questions using lattice and molecular dynamics to calculate dynamic structure factors and thermal transport properties of a-Si. Our analysis supports a qualitatively different picture of atomic vibrations in a-Si from the conventional one in which propagating elastic waves dominate the thermal conduction and are scattered by local variations in elastic modulus rather than anharmonicity. Our work provides strong evidence that, unintuitively, elastic waves with frequencies up to around 10 THz carry substantial heat in disordered media and demonstrates that manipulating local elastic modulus variations is a promising route to realize amorphous materials with extreme thermal properties.

II. COMPUTATIONAL APPROACH

We used lattice and molecular dynamics to examine the atomic vibrations of various amorphous domains. The molecular dynamics calculations were performed using the large-scale atomic/molecular massively parallel simulator (LAMMPS) with a time step of 0.5 fs [14]. Periodic boundary conditions were imposed and the Stillinger-Weber interatomic potential was used [15]. The initial structure we considered contained

*aminnich@caltech.edu

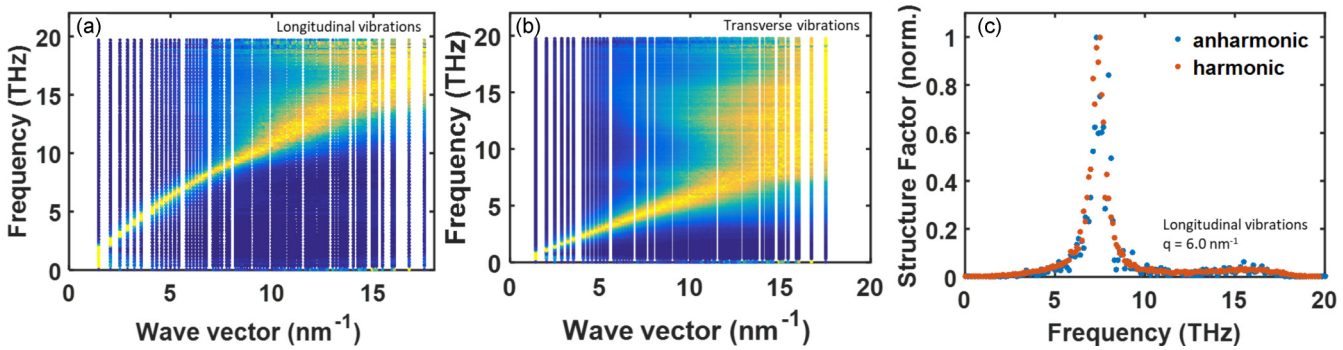

FIG. 1. Dynamical structure factor for (a) longitudinal waves and (b) transverse waves for 4096-atom pure a-Si domain. Bright yellow indicates a high intensity of vibrations with the given frequency and wave vector. A clear phonon band is observed up to around 10 THz despite the atomic disorder. (c) Constant wave vector slice of the dynamical structure factor at $q = 6.0$ nm^{-1} in the longitudinal direction. Anharmonic broadening is negligible at 300 K.

4096 atoms and was created by first melting crystalline silicon at 3500 K for 500 ps in an NVT ensemble. Next, the liquid silicon was quenched to 1000 K with the quench rate of 100 K/ps. The structures were annealed at 1000 K for 25 ns to reduce metastabilities [16]. Finally, the domain was quenched at a rate of 100 K/ps to 300 K and equilibrated at 300 K for 10 ns in an NVT ensemble using a Nose-Hoover thermostat. The structure was then equilibrated at 300 K for 500 ps in an NVT ensemble. After an additional equilibration in an NVE ensemble for 500 ps, the heat fluxes were computed for 1.6 ns in the same NVE ensemble. We use Green-Kubo theory to compute the thermal conductivity of the structure to be 1.5 W m^{-1}K^{-1}, a value that is consistent with prior works [6,16,17].

We begin our analysis to gain more insight into the vibrations carrying heat by characterizing the propagating nature of the normal modes of vibration of the amorphous domain. A convenient metric for this characterization is the dynamic structure factor, given by

$$S_{L,T}(\boldsymbol{q},\omega) = \sum_{\nu} E_{L,T}(\boldsymbol{q},\nu)\delta(\omega - \omega(\boldsymbol{q} = \boldsymbol{0},\nu)), \qquad (1)$$

where the $\boldsymbol{q}$ is phonon wave vector, ω is frequency, and the summation is over all the modes ν at gamma point. E_L and E_T refer to the longitudinal polarization and transverse polarization and are defined as

$$E_{L,T}(\boldsymbol{q},\nu) = \left| \sum_i u_i^{L,T} e^{i\boldsymbol{q}\cdot\boldsymbol{r}_i} \right|^2, \qquad (2)$$

where the summation is over all atoms indexed by i in the domain and $\boldsymbol{r}_i$ are the equilibrium positions. Here $u_i^L = \hat{\boldsymbol{q}} \cdot \boldsymbol{e}(\nu,i)$ and $u_i^T = \hat{\boldsymbol{q}} \times \boldsymbol{e}(\nu,i)$, where $\hat{\boldsymbol{q}}$ is a unit vector and $\boldsymbol{e}(\nu,i)$ is the eigenvector. The dynamic structure factor is precisely what is measured in scattering experiments to measure dispersion relations in crystals and can be applied to search for plane waves in disordered media.

We calculated the eigenvectors of the 4096 atom structure using the general utility lattice program (GULP) with equilibrated structures from MD [18]. As amorphous Si is isotropic, we average the dynamic structure factor over all wave vectors of the same magnitude. If propagating waves exist despite the atomic disorder, the dynamic structure factor will exhibit a clear phonon band with a dispersion; if propagating waves are not supported, the vibrational modes will appear diffuse without an apparent dispersion.

III. RESULTS

A. Dynamic structure factor

The dynamic structure factor for longitudinal waves is presented in Fig. 1(a). The figure demonstrates that despite the atomic disorder a clear dispersion exists up to frequency as high as 10 THz for longitudinal waves, corresponding to a wavelength of 6.5 Å. In the transverse direction, Fig. 1(b), a clear dispersion with broadening is also observed up to ∼5 THz, with a similar transition wavelength of 6.6 Å . For sufficiently high frequency vibrations with wavelengths comparable to interatomic distances, the structure factor is very broad and identifying plane waves with definite frequency and wave vector is not possible. However, the figure clearly shows that propagating elastic waves comprise a substantial portion of the vibrational spectrum. Specifically, by calculating the density of states of the propagating vibrations with a Debye model, we estimate that about 24% of all modes are propagating waves. Our observation is consistent with prior calculations of dynamical structure factor [6,19] but is inconsistent with prior conclusions that propagons have frequencies less than 2–3 THz in amorphous silicon [3,5–7,17,20].

We also observe that the lines are not narrow but have a clear broadening indicating the presence of a scattering mechanism. In crystals, this broadening is typically due to anharmonic interactions. In the harmonic lattice dynamics calculations of amorphous silicon, anharmonic interactions cannot play any role. Instead, the broadening must be due to fluctuations of the local elastic modulus. To assess how broadening due to elastic fluctuations compares to that from anharmonic interactions, we also calculate dynamic structure factors using velocity outputs from MD at 300 K [21]. The longitudinal dynamic structure factors at $q = 6.0$ nm^{-1} with harmonic and anharmonic forces are depicted in Fig. 1(c), demonstrating that the two are nearly identical. Anharmonic broadening has essentially no effect on the lifetimes and the broadening is solely due to elastic modulus fluctuations. Therefore, the picture that emerges from our calculation of dynamical structural factor of a-Si is a vibrational spectrum that is dominated by elastic waves that

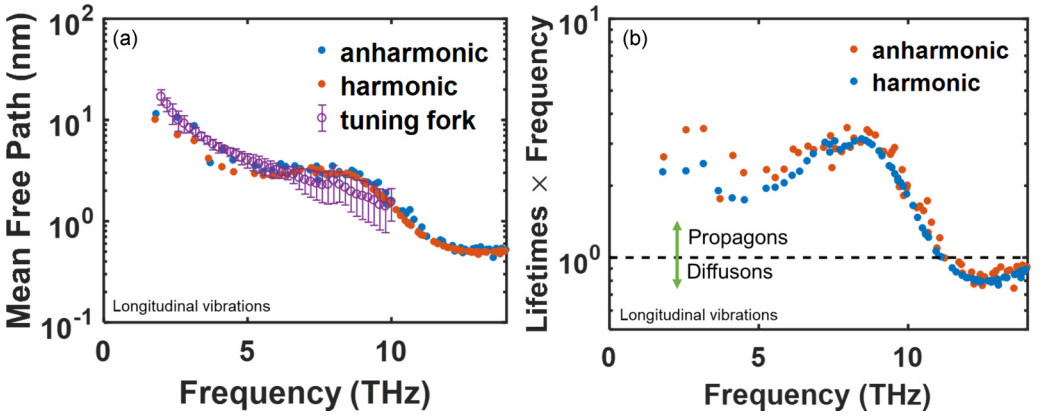

FIG. 2. (a) Spectral mean free path and (b) lifetime multiplied by frequency vs frequency for longitudinal waves with harmonic and anharmonic forces for the 4096-atom pure a-Si domain. We observe an excellent agreement between mean free paths obtained from dynamic structure factors and tuning fork calculations that explicitly simulate the damping of propagating waves. The Ioffe-Regel criterion occurs when lifetime multiplied by frequency equals 1. Propagons are observed up to around 10 THz for longitudinal waves as predicted from the dispersion.

are scattered by elastic modulus variations in the disordered solid.

We next aim to extract quantitative information from the observed broadened lines. Prior works used normal mode analysis to extract lifetimes from molecular dynamics simulations [5,6]. Here, we use the standard scattering theory approach to obtain lifetimes by fitting a constant wave vector slice of the dynamic structure factor with a damped harmonic oscillator (DHO) model [19,21–25]. The lifetime τ at a certain frequency is related to the full width at half maximum Γ by $\tau = 1/\pi\Gamma$ [26]. By multiplying the lifetimes by the group velocity given by the slope of the dispersion, we also obtain mean free paths.

The results are shown in Fig. 2(a). We see that the mean free paths span from 0.5 nm to 10 nm. At still lower frequencies that cannot be included in the present simulations mean free paths are likely even longer, as suggested by experiment [12]. In addition, Fig. 2(b) plots the product of lifetime and vibrational frequency. In this plot, the Ioffe-Regel (IR) crossover from propagons to diffusons, defined as when the lifetime is equal to the period of a wave, can be indicated as a horizontal line [23]. For longitudinal waves, the IR crossover is observed at ∼10 THz and ∼5 THz for transverse waves (not shown); both of these values are in good agreement with the qualitative estimate of the transition frequency from the structure factor.

Having established that propagons comprise a substantial fraction of the vibrational spectrum, we next estimate the propagon contribution to thermal conductivity given knowledge of the linear, isotropic dispersion, the group velocity, and the mean free paths from Figs. 1 and 2 using a Debye model. In this model, we separate the propagon contribution into longitudinal and transverse modes with group velocities obtained from the dispersion as 8000 and 3610 m s^{-1}, respectively. Recalling the bulk thermal conductivity of 1.5 W $m^{-1}K^{-1}$ from the Green-Kubo calculation, we estimate that propagons contribute about 1.35 W $m^{-1}K^{-1}$, or 90% of the thermal conductivity. The primary uncertainty in this estimate is the role of vibrations of frequency less than 2 THz that are challenging to include in both the Green-Kubo and structure factor calculations; however, our conclusion still holds even in the absence of these additional propagating vibrations in our analysis. This contribution is much larger than the values reported previously and suggests that, counterintuitively, heat transport in a-Si is dominated by propagating waves despite the atomic disorder.

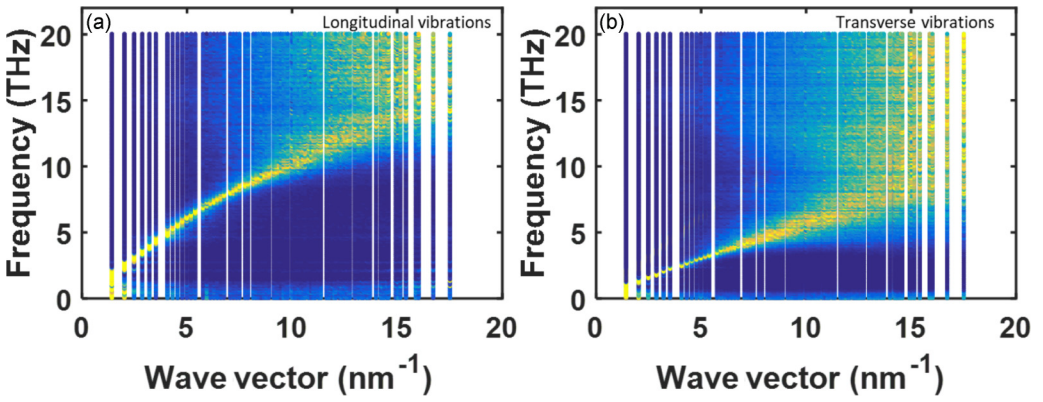

FIG. 3. (a) Dispersion for longitudinal waves and (b) for transverse waves for 4096-atom pure a-Si domain using Tersoff potential from dynamic structure factor calculations. Bright yellow indicates a high intensity of vibrations with the given frequency and wave vector. A clear phonon band is observed up to around 10 THz for longitudinal and 5 THz for transverse directions.

TABLE I. Thermal conductivity comparison for a-Si at 300 K using Tersoff potential without the quantum correction in the specific heat.

Source	Thermal conductivity (W $m^{-1}K^{-1}$)
This work (GK)	2.32 ± 0.30
This work (SF+AF)	2.61
He *et al.* (GK) [5]	2.4 ± 0.35
Lv and Henry (GK) [17]	2 ± 0.32
Lv and Henry (GKMA) [17]	1.75

B. Calculations using Tersoff potential

In addition to the SW potential to describe the interatomic interactions in a-Si, we have calculated thermal conductivity values from the GK formalism and dynamic structure factors using the Tersoff potential. Figure 3 shows the dispersion of longitudinal and transverse directions using the Tersoff potential [27] for 4096 atoms from dynamic structure factor calculations. As observed in the dispersions for the Stillinger-Weber potential, we see clear and well-defined phonon bands up to around 10 THz and 5 THz for longitudinal and transverse directions, respectively. The Ioffe-Regel crossover frequencies using Tersoff potential and the lifetimes from the structure factor agree well with those from Stillinger-Weber potential calculations.

The thermal conductivity of amorphous silicon was then calculated using the Debye model with longitudinal sound velocity of 8179 m/s and transverse sound velocity of 4198 m/s for the propagons from the structure factors (SF) and Allen and Feldman (AF) diffusivities for diffusons and is tabulated among the works by He *et al.* and Lv and Henry as shown in Table I [5,17]. For the frequency range between longitudinal and transverse Ioffe-Regel frequencies, we multiplied a factor of $2/3$ to the Allen and Feldman diffusivities to account for transverse vibrations only. We see that our thermal conductivity prediction from structure factor and Allen and Feldman diffusivities agree well with the available data. About 90% of thermal conductivity is calculated to be from propagons and the rest from diffusons. Calculations using the Tersoff potential also confirm that propagons dominate the thermal conduction in amorphous materials as predicted by our calculations using the Stillinger-Weber potential.

C. Triggered wave analysis

We provide further support for our conclusions with two additional calculations. First, we explicitly demonstrate the propagating nature of vibrational modes by conducting a "tuning fork experiment" in which imposed oscillatory atomic motions at one edge of the atomic domain trigger a longitudinal wave through the a-Si. To perform this calculation, we first create a domain by repeating the 4096-atom cell 10 times along one direction, resulting in a supercell of size $4.3 \times 4.3 \times 43$ nm. In the long dimension, the domain is divided into 80 slabs of width 5.431 Å. Periodic boundary conditions are applied and the temperature is set at 0.1 K to avoid additional thermal displacements. The calculation begins by rigidly displacing the first slab in the longitudinal direction for 2 ps with a sinusoidal wave with amplitude 0.01 Å and a specified frequency ranging from 2 to 10 THz. We computed the longitudinal displacements of every atom for time durations less than 2 ps to prevent edge effects, and subsequently averaged the atomic displacements within each slab.

The wave propagation in a-Si at different frequencies is shown in Fig. 4. It is apparent that waves do indeed propagate through a-Si at 3 THz and 8 THz as predicted by the dynamic structure factor calculations. We obtain mean free paths from these simulations by identifying the location at which the wave amplitude has decreased to $1/e$ of its original value. These mean free paths are in quantitative agreement with those from dynamic structure factor calculations as shown in Fig. 2(a). On the other hand, the excited wave at 16 THz is damped very quickly, and by the second slab the amplitude is already less than $1/e$ of the original value. This observation indicates that at 16 THz the vibration is nonpropagating. Therefore, the "tuning fork experiment" explicitly confirms that longitudinal propagating waves exist up to a high frequency of around 10 THz in a-Si.

D. Role of elastic fluctuations

Second, we examine how the thermal conductivity is affected by the partial elimination of elastic modulus fluctuations. If our assertion regarding scattering by elastic fluctuations is true, we should observe a marked increase in thermal conductivity when these fluctuations are partially

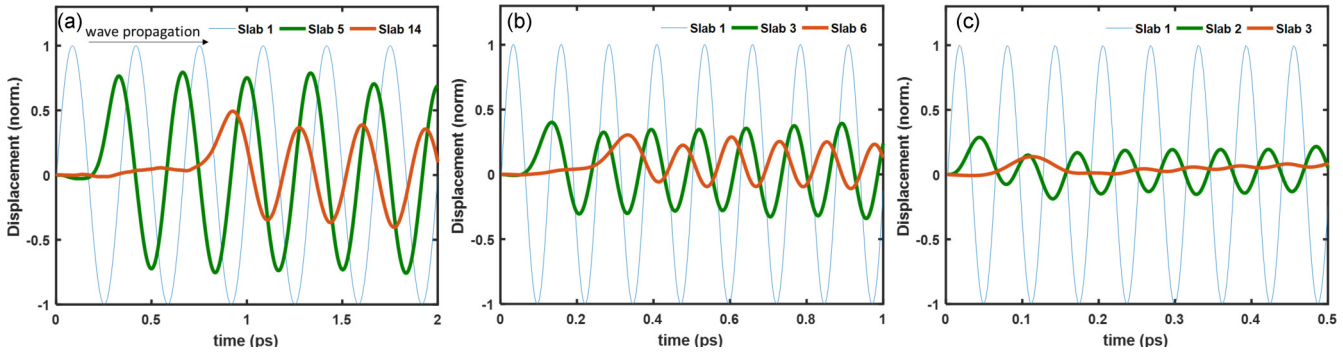

FIG. 4. Temporal displacement of atoms in each slab with triggering frequencies (a) 3 THz, (b) 8 THz, and (c) 16 THz in the longitudinal direction. Each sinusoidal wave represents the averaged displacements of the atoms in a slab. By observing where the amplitudes of the displacement decrease by $1/e$, we estimate that the mean free paths are around 9 and 2 nm for 3 THz and 8 THz waves, respectively. The mean free path of the 16 THz wave is comparable to the interatomic spacing and hence the vibration is nonpropagating.

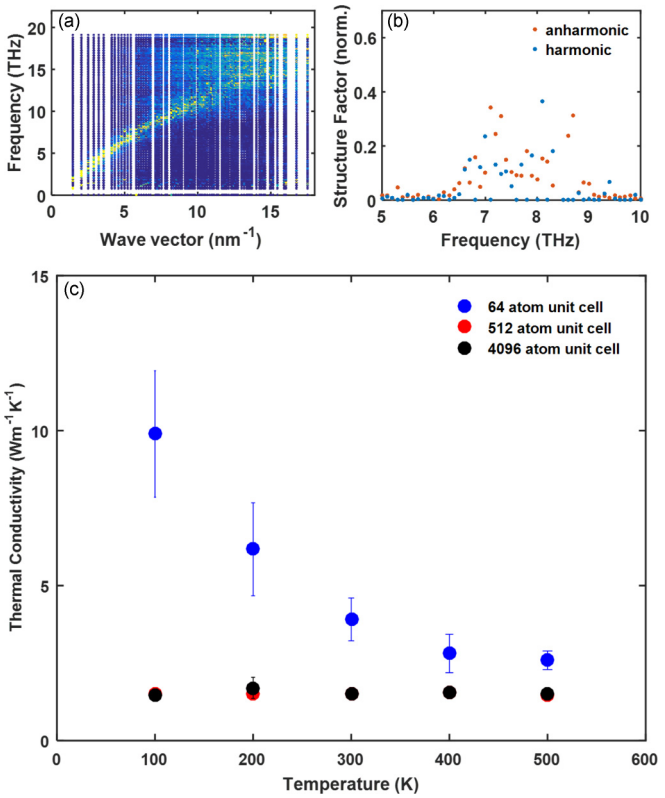

FIG. 5. (a) Dynamic structure factor for longitudinal vibrations for the 64 AUC tiled structure. (b) Constant wave vector slice of the dynamical structure factor at $q = 6.0$ nm^{-1} with harmonic and anharmonic forces for the 64 AUC structure. While the harmonic calculation indicates the presence of closely spaced, discrete modes as occurs in crystals, the anharmonic case exhibits a single broadened mode due to phonon-phonon interactions. (c) Thermal conductivity vs temperature for three amorphous structures. No temperature dependence is observed for 512- and 4096-atom AUC structures, while a noticeable dependence in temperature for the 64-atom AUC tiled structure is evident.

eliminated along with a temperature dependence of thermal conductivity that reflects the renewed dominance of phonon-phonon interactions. To test this hypothesis, we generated two additional domains designed to possess reduced elastic fluctuations consisting of 512- and 64-atom amorphous unit cell (AUC) tiled to create 4096-atom structures. The 512 and 64 AUC domains were created using the same melt-quench procedure described earlier. Elastic fluctuations over a length scale equal to the AUC domain size should be eliminated because the same unit cell is tiled repeatedly in space to form the 4096 atom final structure.

We followed the same procedure as described earlier to obtain dynamic structure factors for the tiled structures. The structure factor for the 512-atom AUC tiled structure appears almost identical to that of the original calculation (not shown). That for the 64-atom AUC tiled structure are shown in Fig. 5(a). We observe discrete points rather than a continuous broadening, indicative of the dynamic structure factor having delta-function-like peaks as occurs in c-Si. From a constant wave vector slice of the dynamic structure factor for the 64-atom AUC tiled structure in Fig. 5(b), we observe that anharmonicity broadens those individual peaks of the modes from the harmonic calculations, indicating that anharmonicity plays a role in scattering these modes. Overall, these calculations indicate that the 64-atom AUC structure possesses vibrations that are characteristic of a semicrystalline solid while the 512-atom AUC remains effectively amorphous.

We now compute the thermal conductivity of the three structures using Green-Kubo theory. The resulting thermal conductivity calculations of these structures are shown in Fig. 5(c). The figure shows that the pure a-Si and the 512-atom AUC tiled structure have identical thermal conductivity with little temperature dependence. This result confirms that the 512-atom AUC structure is effectively amorphous. However, we observe a significant increase in thermal conductivity of the 64-atom AUC tiled structure, by more than a factor of 2 at room temperature, along with a marked temperature dependence. At 100 K, the thermal conductivity of the 64-atom AUC tiled structure is $\sim$10 W m^{-1}K^{-1}, more than six times that of 4096 AUC structure. Therefore, the 64-atom AUC tiled structure exhibits characteristics of crystals, and the key disorder length scale that sets the transition of thermal vibrations from crystalline to amorphous character lies between 10 and 20 Å.

IV. DISCUSSION

Our analysis differs from prior works in two key respects. First, we use a standard definition of lifetime from scattering theory as the broadening of the inelastic peak of the structure factor rather than the typical normal-mode lifetime. Although the normal-mode and structure factor definitions coincide at frequencies below around 2 THz [6], they do not agree at higher frequency. Our tuning fork analysis explicitly shows that the physical lifetime corresponding to the damping of a wave is given by the lifetime from the structure factor. Those given by normal-mode analysis give lifetimes that are 3 to 10 times higher than those observed in the tuning fork calculation.

Second, we determine the propagon-diffuson transition frequency using the standard Ioffe-Regel criterion with the lifetimes from the structure factor, leading to transition frequencies of around $\sim$5 THz and $\sim$10 THz for transverse and longitudinal vibrations, respectively. Prior works used different criteria to identify propagon-diffuson transition frequency, such as the frequency at which diffusivities calculated by different methods are equal [6], leading to the commonly cited transition frequency of 2–3 THz. Our tuning fork analysis in Figs. 2 and 4 explicitly shows that modes that were previously considered to be diffusons by the latter criterion are in fact propagating. Our conclusion that propagons dominate thermal conduction in amorphous Si is a direct and unavoidable consequence of these observations.

The picture of a gas of delocalized elastic vibrations transporting heat in amorphous solids suggests follow-on experiments as well as new strategies to realize exceptional thermal materials. First, our prediction of propagons existing up to around 10 THz can be verified with additional thermal measurements on amorphous nanostructures with characteristic dimensions of less than 10 nm as well as with scattering methods such as inelastic x-ray scattering. Second, our analysis suggests that fully dense solids with exceptionally low thermal conductivity can be achieved by disrupting the propagating

modes via enhancement of variations of local elastic modulus, expanding the physical range of thermal conductivity of solids.

V. CONCLUSIONS

In summary, we have examined the atomic vibrations in *a*-Si using lattice and molecular dynamics calculations. Our study reveals a qualitatively different view of atomic vibrations in *a*-Si from a conventional one in which propagating elastic waves dominate the thermal conduction and are scattered by elastic fluctuations instead of anharmonicity. Our work provides important insights into the long-standing problem of thermal transport in disordered solids.

ACKNOWLEDGMENTS

This work was supported by the Samsung Scholarship, NSF CAREER Award No. CBET 1254213, and the Resnick Fellowship from the Resnick Sustainability Institute at Caltech.

[1] M. C. Foote, M. Kenyon, T. R. Krueger, T. A. McCann, R. Chacon, E. W. Jones, M. R. Dickie, J. T. Schofield, D. J. McCleese, and S. Gaalema (unpublished).
[2] M. C. Wingert, J. Zheng, S. Kwon, and R. Chen, Thermal transport in amorphous materials: A review, Semicond. Sci. Technol. **31**, 113003 (2016).
[3] P. B. Allen, J. L. Feldman, J. Fabian, and F. Wooten, Diffusons, locons and propagons: Character of atomic vibrations in amorphous Si, Philos. Mag. B **79**, 1715 (1999).
[4] J. L. Feldman, M. D. Kluge, P. B. Allen, and F. Wooten, Thermal conductivity and localization in glasses: Numerical study of a model of amorphous silicon, Phys. Rev. B **48**, 12589 (1993).
[5] Y. He, D. Donadio, and G. Galli, Heat transport in amorphous silicon: Interplay between morphology and disorder, Appl. Phys. Lett. **98**, 144101 (2011).
[6] J. M. Larkin and A. J. H. McGaughey, Thermal conductivity accumulation in amorphous silica and amorphous silicon, Phys. Rev. B **89**, 144303 (2014).
[7] W. Lv and A. Henry, Examining the validity of the phonon gas model in amorphous materials, Sci. Rep. **6**, 37675 (2016).
[8] D. G. Cahill, M. Katiyar, and J. R. Abelson, Thermal conductivity of *a*-Si: H thin films, Phys. Rev. B **50**, 6077 (1994).
[9] R. Sultan, A. D. Avery, J. M. Underwood, S. J. Mason, D. Bassett, and B. L. Zink, Heat transport by long mean free path vibrations in amorphous silicon nitride near room temperature, Phys. Rev. B **87**, 214305 (2013).
[10] B. L. Zink, R. Pietri, and F. Hellman, Thermal Conductivity and Specific Heat of Thin-Film Amorphous Silicon, Phys. Rev. Lett. **96**, 055902 (2006).
[11] J. L. Braun, C. H. Baker, A. Giri, M. Elahi, K. Artyushkova, T. E. Beechem, P. M. Norris, Z. C. Leseman, J. T. Gaskins, and P. E. Hopkins, Size effects on the thermal conductivity of amorphous silicon thin films, Phys. Rev. B **93**, 140201 (2016).
[12] S. Kwon, J. Zheng, M. C. Wingert, S. Cui, and R. Chen, Unusually high and anisotropic thermal conductivity in amorphous silicon nanostructures, ACS Nano **11**, 2470 (2017).
[13] X. Liu, J. L. Feldman, D. G. Cahill, R. S. Crandall, N. Bernstein, D. M. Photiadis, M. J. Mehl, and D. A. Papaconstantopoulos, High Thermal Conductivity of a Hydrogenated Amorphous Silicon Film, Phys. Rev. Lett. **102**, 035901 (2009).
[14] S. Plimpton, Fast parallel algorithms for short-range molecular dynamics, J. Comput. Phys. **117**, 1 (1995).
[15] F. H. Stillinger and T. A. Weber, Computer simulation of local order in condensed phases of silicon, Phys. Rev. B **31**, 5262 (1985).
[16] J. Moon and A. J. Minnich, Sub-amorphous thermal conductivity in amorphous heterogeneous nanocomposites, RSC Adv. **6**, 105154 (2016).
[17] W. Lv and A. Henry, Direct calculation of modal contributions to thermal conductivity via Green-Kubo modal analysis, New J. Phys. **18**, 013028 (2016).
[18] J. D. Gale, GULP: A computer program for the symmetry-adapted simulation of solids, J. Chem. Soc., Faraday Trans. **93**, 629 (1997).
[19] Y. M. Beltukov, C. Fusco, D. A. Parshin, and A. Tanguy, Boson peak and Ioffe-Regel criterion in amorphous siliconlike materials: The effect of bond directionality, Phys. Rev. E **93**, 023006 (2016).
[20] H. Reza Seyf and A. Henry, A method for distinguishing between propagons, diffusions, and locons, J. Appl. Phys. **120**, 025101 (2016).
[21] H. Shintani and H. Tanaka, Universal link between the boson peak and transverse phonons in glass, Nat. Mater. **7**, 870 (2008).
[22] S. M. Shapiro, J. D. Axe, G. Shirane, and T. Riste, Critical Neutron Scattering in $SrTiO_3$ and $KMnF_3$, Phys. Rev. B **6**, 4332 (1972).
[23] S. N. Taraskin and S. R. Elliott, Low-frequency vibrational excitations in vitreous silica: The Ioffe-Regel limit, J. Phys.: Condens. Matter **11**, A219 (1999).
[24] G. T. Barkema and N. Mousseau, High-quality continuous random networks, Phys. Rev. B **62**, 4985 (2000).
[25] T. Damart, V. M. Giordano, and A. Tanguy, Nanocrystalline inclusions as a low-pass filter for thermal transport in *a*-Si, Phys. Rev. B **92**, 094201 (2015).
[26] G. Nilsson and G. Nelin, Phonon dispersion relations in Ge at 80 K, Phys. Rev. B **3**, 364 (1971).
[27] J. Tersoff, Empirical interatomic potential for silicon with improved elastic properties, Phys. Rev. B **38**, 9902 (1988).